

Path Planning and Guidance Laws of a Formula Student Driverless Car

Solange Dolores Rebocho dos Santos

solange.santos@tecnico.ulisboa.pt

Instituto Superior Técnico, Universidade de Lisboa, Lisboa, Portugal

November 2021

Abstract: Autonomous driving has been a topic of great interest in several areas, from which motor racing is no exception. Aiming to autonomously control the future Formula Student Lisboa vehicle, this work was developed with the objective of implementing different strategies for control and path planning. These strategies were tested in simulation, using a realistic model of the prototype. For planning, as it is important in competition to minimise the time, the necessary references were generated with this in mind. The approach followed involves the decoupling of the lateral and longitudinal subsystems, where the reference path was obtained using artificial potential fields and then combined with a two passes algorithm developed to generate a speed profile. This allowed to obtain a sub-optimal solution that adequately portrays the expected behavior of a human driver while respecting traction conditions. Following this approach, the process of generating the speed reference requires prior knowledge of the track layout. However, another approach was developed, without this premise being verified for obstacle avoidance i.e, for a scenario where, in addition to the track limits, there is the presence of static obstacles. For control, a decoupled approach was followed once again, controlling each one of the subsystems individually. With guidance as main focus, several strategies were implemented for lateral control and only one for longitudinal control.

Keywords: Formula Student, autonomous driving, path planning, obstacle avoidance, guidance laws, automotive control

I. INTRODUCTION

Autonomous vehicles have been a topic of growing research and investment in recent decades. Such vehicles can have a wide range of applications covering different types of systems, like small unguided robots or unmanned vehicles, and environments, which can be extended from indoors to outdoors or even to planetary exploration.

Focusing on driverless cars, the control design for autonomous driving and racing has attracted considerable attention which led to the creation of different types of competitions. In a more academic oriented environment, the Formula Student (FS) is one of the most well-known, where students are challenged to design, build and test a race car according to a specific set of rules. With the intent of competing in the driverless category, the Formula Student team from Instituto Superior Técnico - Universidade de Lisboa (FST) is currently developing its first hybrid prototype, in the sense that allows both person-driven and driverless configurations.

This autonomy is not just "all or nothing", but rather a spectrum with six development stages defined by the Society of Automotive Engineers (SAE), where the core competencies needed can be broadly divided into three categories, namely perception, planning, and control [19].

Being what allows the vehicle to detect and process the environment, the perception algorithms usually make use of GPS (Global Positioning System), computer vision and a wide range of sensors [24] which, to compensate for individ-

ual shortcomings and achieve a positive redundancy, can be coupled via sensor fusion. From the received data, planning derives instructions for the system to act in accordance with such data, being usually categorized in global, behavioral or local [12], [19], [21]. Regarding this last classification, it may concern obstacle avoidance [8], [15], trajectory planning [11], [12] or path planning [12], [16] where the latter frequently involves a decoupled approach regarding the steering and the velocity. Finally, control competency executes the planned actions that have been generated by the previous process. Considering the decoupling, this execution is achieved by two different controllers, commonly designated as lateral and longitudinal controllers, giving two different input signals: a steering command; and an acceleration or a braking signal, respectively.

However, the complexity of the underlying algorithms associated with each one of the mentioned categories is highly influenced by the scenario where the vehicle will be inserted. Comparing autonomous city driving with autonomous racing, the degree of unpredictability of the surroundings in the latter is distinctly lower which, combined with the highly controlled and regulated environment, allows for simpler approaches regarding perception that frequently rely on the combination of LiDAR (Light Detection and Ranging) sensors, cameras and computer vision [1], [13]. The planning, is usually based on a minimum lap time problem, which accounts for the vehicle dynamics and track boundaries. Lastly, the control

strategies used in a racing scenario, frequently require more data than provided by perception, which can be acquired from motor encoders, GPS or accelerometer, for example, or from estimation [13]. The longitudinal control problem is frequently simplified by assuming that many of the dynamics of the drivetrain, motors and transmission is regulated by low-level controllers, resulting in a fairly simple system to control [6], or combined with the lateral control for an appropriate MPC (Model Predictive Control) formulation [16], [22]. On the other hand, lateral control tends to include the inertia of the car and tire forces, ranging from models based in the path, which may [22] or may not [20] involve MPC formulation, to models based on vehicle dynamics like the single-track [14] or four-wheeled [20] models.

Being this work mainly focused in planning and lateral control of the autonomous vehicle pipeline, the objectives are threefold:

- Develop an algorithm for path planning under the assumptions that there is an *a priori* knowledge of the track layout and an algorithm for obstacle avoidance considering static obstacles;
- Design different control strategies to effectively steer the vehicle, as well as a low-level controller, in order to obtain more accurate results, ensure vehicle stability and avoid wheel lock or spin;
- Test, evaluate and compare the different algorithms with a developed realistic model of the vehicle.

The remainder of this work is structured as follows: Section II describes the vehicle modelling, Section III the planning algorithms and Section IV the control strategies; the simulation results will be presented and discussed in Section V and the conclusions, as well as suggestions for future research on this topic, will be covered in Section VI.

II. VEHICLE MODELLING

Since the controller design, tuning and validation processes are made resorting to simulation, it is important to develop models that emulate the vehicle behaviour. In this section, two categories of vehicle models are detailed: the first, designated as realistic, has a high degree of complexity, being used for simulation; the second, designated as simplified, includes the models used for control and observer design as well as for preliminary validation.

A. Realistic Model

The vehicle model used for simulation has six degrees of freedom (DOF), modelling the vehicle as a rigid body with a simplified vertical suspension system for each wheel. The car is four-wheel-driven (4WD) by independent electric motors and front-wheel steered.

The model formulation is done resorting to a state-space representation where the states are the linear \mathbf{v} and angular $\mathbf{\Omega}$ velocities of the center of gravity (CG) expressed in the local frame, the CG position \mathbf{p}_{CG} expressed in the global frame,

the Euler angles Φ associated with the rotations from global to local frame and the angular speeds of each wheel ω . Having as inputs the wheel torques \mathbf{t}_w and the steering angles δ , the model returns the state derivatives and generates as output the suspension deformations Δ_z , the slip ratio κ , the slip angles α and the forces \mathbf{f}_x , \mathbf{f}_y , \mathbf{f}_z and moments \mathbf{m}_z resulting from the tire-ground interaction.

Regarding the kinematics, the linear and angular velocities of the body frame can be expressed in the global frame as [5]

$$\dot{\mathbf{p}}_{CG} = \mathbf{S}^\top \mathbf{v} \quad (1)$$

$$\dot{\Phi} = \mathbf{R}^{-1} \mathbf{\Omega} \quad (2)$$

where \mathbf{R} stands for the transformation matrix from the Euler angles rate of change to the CG angular velocities and \mathbf{S} is the rotation matrix that converts global frame coordinates into local frame coordinates. The expressions for both matrices can be found in [5].

Lastly, with respect to dynamics, from the Newton-Euler equations the following equations can be obtained [5]

$$m\dot{\mathbf{v}} = -m(\mathbf{\Omega} \times \mathbf{v}) + m \mathbf{S} \mathbf{g} + \mathbf{f}_{CG} \quad (3)$$

$$\mathbf{J} \dot{\mathbf{\Omega}} = -(\mathbf{\Omega} \times \mathbf{J} \mathbf{\Omega}) + \mathbf{t}_{CG} \quad (4)$$

$$J_w \dot{\omega} = T_w - F_x R - T_{dis_w} \quad (5)$$

where m is the vehicle mass, \mathbf{g} the gravity vector, \mathbf{J} and J_w are the vehicle's inertia tensor and wheel rotational inertia, respectively, and R the tire radius. In the above equations, the terms with the subscript CG represent the resultant force and torque acting on the CG, which includes tire, dissipation and aerodynamics forces in (3) and energy dissipation in (4). In equation (5), T_{dis_w} stands for dissipation torque. All dissipations and aerodynamics forces were modeled in a quadratic form.

Powertrain

Due to the complexity of modeling the full powertrain system, a simplification was made in which the motor losses were dynamically modeled, resorting to the implementation of an efficiency map and all the remaining losses were considered as constant. Additionally, to approximate the torque response dynamics, the first order system

$$T = \frac{\eta_{PT}}{\tau_{PT}s + 1} T_{cmd} \quad (6)$$

was implemented, where η_{PT} is an efficiency to account for the remaining losses and τ_{PT} is the time constant for the torque dynamics that accounts for the electrical time constant and mechanical response. This model was inherent from [4].

Steering

Considering a low-speed or low curvature cornering manoeuvre, as the vehicle travels along the curved path, all tires follow unique trajectories around a shared turn center, each one with a specific curvature radius. Hence, to avoid sliding and maintain a pure rolling condition, the angle described by the inside front tire angle must be larger than the one described by the outside front tire.

The geometry that allows to obtain such configuration, known as Ackermann steering, computes the steering angles as

$$\delta_{FR} = \arctan \left(\frac{L \tan(\delta)}{L - \frac{L_W}{2} \tan(\delta)} \right) \quad (7a)$$

$$\delta_{FL} = \arctan \left(\frac{L \tan(\delta)}{L + \frac{L_W}{2} \tan(\delta)} \right) \quad (7b)$$

in which $L = L_F + L_R$ and L_W are the wheelbase (sum of the distances from the CG to the front axle L_F and from the CG to the rear axle L_R) and the track width (distance between two wheels of the same axle) respectively. This geometry was the one considered since low-speed or low curvature cornering manoeuvre are typically found in FS race tracks [4].

Similarly to the powertrain modelling, a first-order system given by

$$\delta = \frac{1}{\tau_{SA}s + 1} \delta_{cmd} \quad (8)$$

was used in order to model the relation between the real and command steering angles. In such model τ_{SA} stands for the steering actuation time constant. Lastly, a slew rate limitation was also implemented to model the physical limit in the actuator velocity.

Tires

The tires, as the only element interacting with the driving surface, are the ones responsible for the generation of the forces and moments that allow the acceleration, braking and turning of the vehicle. Due to the inherent complexity of measuring such mechanical quantities in real time, tire models are commonly used to provide estimations.

For this work, the Pacejka tire model [18] was considered to be suitable as it is the one used by the FST Lisboa tire supplier. However, to be able to employ the provided tire model and compute the friction loads, several concepts must be defined first.

When a vehicle is in contact with the ground, part of the energy delivered by the motor torque is consumed by friction, generating an longitudinal force F_x which, opposing the wheel rotation, is responsible for the acceleration and braking of the vehicle. This force is influenced by the slip phenomenon, which can be quantified by the slip ratio:

$$\kappa = \frac{\omega R - v_{w_x}}{v_{w_x}} \quad (9)$$

in which v_{w_x} represents the longitudinal component of the linear wheel velocity \mathbf{v}_w in the wheel coordinate system. However, it is important to note that, if the vehicle is turning, a lateral force F_y is also generated, which is influenced not by the longitudinal slip, but by the side slip, quantified by the angle presented in (10).

$$\alpha = \arctan \left(\frac{v_{w_y}}{v_{w_x}} \right) \quad (10)$$

Given the non-uniform tire deformation that occurs in the surface originated by the tire-ground interaction, not only

forces but also moments are generated, like the self-alignment moment M_z , which depends on the same parameters as the lateral force since it is generated by it.

Having been defined the concepts associated with tire mechanics, it is now possible to state the formula inherent to the chosen model. Commonly known as the Magic Formula, this model resorts to a semi-empirical formulation [18], which is present in (11), to mathematically describe not only both longitudinal and lateral forces, but also the self-alignment moment.

$$Y_{MF} - S_V = D \sin \left(C \arctan \left((1 - E) B (x_{MF} + S_H) + E \arctan (B (x_{MF} + S_H)) \right) \right) \quad (11)$$

Regarding the parameters inherent to (11), B , C , D and E are the stiffness factor, shape factor, peak value and curvature factor, respectively, which are empirically obtained and must respect the relations presented in [18]; S_V and S_H are the vertical and horizontal shifts and, lastly, X_{MF} and Y_{MF} are the input (which can be either κ or α) and output (which can be F_x , F_y or M_z) variables, respectively.

B. Simplified Models

As it can be seen from the previous subsection, the equations of motion are complex and highly nonlinear, which would lead to a complex deduction of the appropriate controllers or estimators. As such, two simplified models were used, which will be presented next.

Bicycle Dynamics Model

In order to develop a model and understand the dynamic involved, the balance of forces and moments plays an important role. Assuming that the vehicle can be seen as a rigid body with planar motion, is rear-wheel driven (RWD) and front steered only, from the lumping of the two wheels belonging to the same axis (inherent to the bicycle model formulation) the dynamics can be described by [4]

$$\dot{v}_x = \frac{1}{m} \left(-F_y^F \sin(\delta) + F_x^R \right) + v_y \dot{\psi} \quad (12)$$

$$\dot{v}_y = \frac{1}{m} \left(F_y^F \cos(\delta) + F_y^R \right) - v_x \dot{\psi} \quad (13)$$

$$\ddot{\psi} = \frac{1}{I_{zz}} \left(L_F F_y^F \cos(\delta) - L_R F_y^R \right) \quad (14)$$

where the tire forces F_x and F_y were modelled resorting to the simplified Magic Formula [13].

For control and estimator design, a linearisation of (12) and (14) was performed. Considering C_{α_F} and C_{α_R} the cornering stiffness of the front and rear tires and (X, Y) the position of the vehicle reference point, in the fixed frame, obtained from the integration of [3]

$$\dot{X} = v_x \cos(\psi) - v_y \sin(\psi) \quad (15)$$

$$\dot{Y} = v_x \sin(\psi) + v_y \cos(\psi) \quad (16)$$

a state space model can be formulated for the lateral subsystem where the states are $[Y \ \psi \ v_y \ \dot{\psi}]^\top$ and the dynamic matrix \mathbf{A} and the input vector \mathbf{B} are

$$\begin{bmatrix} 0 & v_x & 1 & 0 \\ 0 & 0 & 0 & 1 \\ 0 & 0 & -\frac{2(C_{\alpha_F} + C_{\alpha_R})}{mv_x} & -\frac{2(C_{\alpha_R}L_R - C_{\alpha_F}L_F)}{mv_x} \\ 0 & 0 & -\frac{2(C_{\alpha_R}L_R - C_{\alpha_F}L_F)}{I_{zz}v_x} & -\frac{2(C_{\alpha_F}L_F^2 + C_{\alpha_R}L_R^2)}{I_{zz}v_x} \end{bmatrix} v_x + \begin{bmatrix} 0 & 0 & \frac{2C_{\alpha_F}}{m} & \frac{2L_FC_{\alpha_F}}{I_{zz}} \end{bmatrix}^\top$$

Bicycle Dynamics Model in Terms of Road Errors

A dynamics model, with the lateral position and the yaw angle as degrees of freedom was presented in the previous section. However, it can be useful to define a dynamics model in terms of position and heading errors with respect to the road. To formulate such model it is only necessary to redefine the linear equations obtained from the previous state space model in terms of the mentioned errors.

Since the inertial acceleration of the vehicle a_y have the contribution of two terms, namely, the acceleration \dot{v}_y due to motion along the y axis and the centripetal acceleration $v_x\dot{\psi}$, assuming steady-state conditions allows to obtain the desired acceleration as in (17) [20] where $\dot{\psi}_d$ can be obtained from the under-steer gradient K_u and wheelbase L through (18) [2].

$$\dot{a}_{y_d} = v_x\dot{\psi}_d \quad (17)$$

$$\dot{\psi}_d = \frac{v}{L + K_u v^2} \delta \quad (18)$$

With these variables defined, the errors in the lateral and yaw accelerations can be computed as [20]

$$\ddot{e}_y = a_y - a_{y_d} = \dot{v}_y + v_x(\dot{\psi} - \dot{\psi}_d) \quad (19)$$

$$\ddot{e}_\psi = \dot{\psi} - \dot{\psi}_d \quad (20)$$

Substituting (19), (20) and (18) in in the equations of the previous model (neglecting both K_u and v_y which simplifies (18)) a linear state space can be finally obtained [20] where the state are $[e_y \ \dot{e}_y \ e_\psi \ \dot{e}_\psi]^\top$ and the dynamic matrix \mathbf{A} and the input vector \mathbf{B} are

$$\begin{bmatrix} 0 & 1 & 0 & 0 \\ 0 & -\frac{2(C_{\alpha_F} + C_{\alpha_R})}{mv_x} & \frac{2(C_{\alpha_F} + C_{\alpha_R})}{m} & \frac{2(C_{\alpha_R}L_R - C_{\alpha_F}L_F)}{mv_x} \\ 0 & 0 & 0 & 1 \\ 0 & -\frac{2(C_{\alpha_F}L_F + C_{\alpha_R}L_R)}{I_{zz}v_x} & \frac{2(C_{\alpha_F}L_F - C_{\alpha_R}L_R)}{I_{zz}} & \frac{2(C_{\alpha_R}L_R^2 - C_{\alpha_F}L_F^2)}{I_{zz}v_x} \end{bmatrix} + \begin{bmatrix} 0 & \frac{2C_{\alpha_F}}{m} - \frac{2(C_{\alpha_F}L_F - C_{\alpha_R}L_R)}{mL} - \frac{v_x^2}{L} & 0 & \frac{2C_{\alpha_F}L_F}{I_{zz}} - \frac{2(C_{\alpha_F}L_F^2 + C_{\alpha_R}L_R^2)}{I_{zz}L} \end{bmatrix}^\top$$

III. PLANNING ALGORITHMS

Being this work focused on local planning, in this section the algorithms developed for path planning and obstacle avoidance will be presented.

A. Path Planning

For path planning the employed strategy consists in a decoupled approach, in the sense that one algorithm obtains the path, accounting for the boundaries of the track, and another one regulates its speed. Both algorithms will be described next.

Reference Path

Aiming for a more optimised reference path than the centerline, which is the common baseline solution, the potential field concept resorting to virtual forces was used. The main idea behind this approach consists in considering the vehicle as a charged particle moving under the influence of repulsive and attractive potentials. Since the objective is maintain the vehicle within the track, the repulsive forces will be associated with the track boundaries, the attractive force with a target ahead and the guidance with the result of the combination of both effects.

The computation of the attractive force is quite simple as it only requires the knowledge of the actual position of the car \mathbf{p} and the selection of a target point lying on the centerline \mathbf{p}_{target} . This force can be mathematically described as [23]

$$\mathbf{f}_{att} = K_{att}(\mathbf{p}_{target} - \mathbf{p}) \quad (21)$$

where K_{att} is a gain, simulating a proportional controller.

The repulsive force, on the other hand, requires more attention since it depends on the danger level U which is influenced by the danger of the boundary γ and the distance between the vehicle's position and the limits of the track $d(X, Y)$. The danger level U can be given by [23]

$$U = \max_k \lim_{\gamma \rightarrow \gamma_k} \frac{d_k^{1-\gamma}(X, Y) - d_{\max}^{1-\gamma}}{d_{\min}^{1-\gamma} - d_{\max}^{1-\gamma}} \quad (22)$$

where d_{\min} is the distance below which U will be always 1 and d_{\max} the distance above which U will be always 0. Analysing all the boundary points in the proximity of the vehicle, the one with the minimum distance is selected since it will present the higher danger level. From this point \mathbf{p}_{danger} , the repulsive force can be calculated from [23]

$$\mathbf{f}_{rep} = K_{rep} U \frac{\mathbf{p} - \mathbf{p}_{danger}}{\|\mathbf{p} - \mathbf{p}_{danger}\|} \quad (23)$$

where K_{rep} is a gain, as in the attractive force.

Seeing the virtual resultant force \mathbf{f} direction as a desired orientation, as it minimizes the potential, and knowing the current heading of the vehicle ψ , an heading error e_ψ can be defined as shown in Figure 1. The steering command intends to drive this error to 0 meaning that this is a regulator problem; thus, the steering command was set equal to the error. In this way, the vehicle is steered in the direction of the resultant force. This law could seem extremely simple, since it results from a unitary proportional controller, but it should be kept in mind that the reasoning behind the heading error used to obtain this control action involves highly non-linear calculations.

Having in mind that an optimal solution cannot be guaranteed, in the sense of guaranteeing the completion of the course with minimum time, this method was further combined with

the speed algorithm that will be presented next, in order to obtain the set of parameters that will result in a solution close to the optimal. Such set consists on the distance to the target, which will be referenced as offset, K_{rep} and γ . The attractive gain was left out and set to a unitary value since, although it can be seen as parameter, it is related with the offset. The procedure adopted in the search of these parameters was a sweeping in which, for each of the resultant paths obtained for a constant longitudinal speed of $v_x = 5$ [m/s], the speed profile was found and the one with the lowest time was chosen as final.

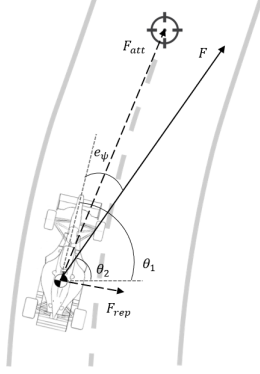


Figure 1. Schematic of the forces felt by the vehicle

Reference Speed

Although approaches capable of simultaneously optimising both the path and the speed profile exist, the procedure taken was based on aiming to find a speed profile that results in complete a given fixed path in minimum time respecting traction conditions and powertrain constraints.

Considering an isotropic tire, the maximum transferable force between the road and the vehicle is limited by the tire force which, using the friction circle model, can be computed from

$$F_x^2 + F_y^2 \leq (\mu F_z)^2 \quad (24)$$

Neglecting the aerodynamic downforce, the forces in (24) are given by

$$F_x = ma_x + \frac{1}{2} \rho A_p C_D v_x^2 = ma_x + F_{dis} \quad (25a)$$

$$F_y = mv_x^2 K \quad (25b)$$

$$F_z = mg \quad (25c)$$

where K stands for the path curvature obtained through

$$K = \frac{X'Y'' - Y'X''}{((X')^2 + (Y')^2)^{\frac{3}{2}}} \quad (26)$$

In (26), the single and double apostrophes denote the first and second derivatives, respectively, of the waypoints coordinates (X, Y) expressed in the global frame. These derivatives can be approximated using forward, backward and central differences in starting, finishing and remaining points, respectively.

Discretising the path at N steps, using a fixed step Δs in arc length s , and performing algebraic manipulation, which can be seen with more detail in [10], of the equations for uniformly accelerated motion

$$v_x(k+1) = v_x(k) + a(k)\Delta t \quad (27a)$$

$$\begin{aligned} s(k+1) &= s(k) + v_x(k)\Delta t + \frac{1}{2}a(k)(\Delta t)^2 \\ &= s(k) + \Delta s \end{aligned} \quad (27b)$$

it is possible to obtain the following equations

$$\Delta s = \frac{v_x^2(k+1) - v_x^2(k)}{2a(k)} \quad (28)$$

$$v_x(k+1) = \sqrt{v_x^2(k) + 2a(k)\Delta s} \quad (29)$$

$$t(k+1) = t(k) + \frac{2\Delta s}{v_x(k+1) + v_x(k)} \quad (30)$$

which will be used in the optimisation process. This optimisation is split into two passes, a backward and a forward one, both explained below. The algorithms of both passes can be found in [10], where the pseudo-code is provided.

→ Backward Pass

In the first pass, the backward algorithm determines the maximum speed in turns and the necessary braking distance before each turn. Starting from the finishing point and iterating the sampled curve in the reverse order, the maximum speed at each step is obtained from the minimum between a user-defined limit v_{xlim} and the maximum speed for the previous sample $(k-1)$, which corresponds to the real positive solution of (24), solved for $K(k-1)$ and $a_x = 0$. Once the speed is computed, the negative acceleration required to achieve such value can be determined with (28) and the minimum between this value and the available by the powertrain, which is given by function h that will be described latter, is applied. Then, the next iteration continues by moving backward along the curve.

→ Forward Pass

In the second pass, the forward algorithm maximises the speed and determines the optimal times of transition between acceleration and braking. This is done reparametrising the originally profile using time steps, instead of distance steps, forming a trajectory parametrised in time [10]. Beginning in the starting point, and iterating in the forward order, when the velocity is below the velocity profile of the backward pass, the maximum available positive acceleration is applied to increase the speed and, once such velocity is reached, the optimal braking is applied as in the previous pass. As a result, the optimal transition times between acceleration and braking are determined to execute the track in the minimum time and under the acceleration constraints resulting from traction and/or powertrain.

→ Powertrain constraint

From the description provided, it can be seen that both passes use a function h to determine the maximum available longitudinal acceleration in direction $d = \pm 1$, with forward

represented as positive. Using K and v_x , such acceleration can be determined from (24) based on the maximum available tire force in the longitudinal direction. However, this value is further limited by the vehicle powertrain [10].

Assuming that the available torque T can be approximated as constant, but differs, however, depending on the axle and on whether the vehicle is braking or accelerating, the wheel tractive force F_{trc} can be computed from [10]

$$F_{\text{trc}} = \frac{1}{R} \sum_{i=1}^{N_{\text{mr}}} (\eta_{i,\text{trans}} \cdot r_{\text{gear}} \cdot T_i) \quad (31)$$

where $\eta_{i,\text{trans}}$ is the transmission efficiency and r_{gear} the gear ratio. Thus, the maximum available longitudinal acceleration can then be given by

$$h = \frac{1}{m} \left[-F_{\text{dis}} + d \min \left(\sqrt{\mu^2 F_z^2 - F_y^2}, |F_{\text{trc}}| \right) \right] \quad (32)$$

B. Obstacle Avoidance

For obstacle avoidance a decoupling between the guidance and acceleration was followed once again, which will be described next. In this scenario, the static obstacles are intended to represent other vehicles which were modelled as rectangles.

Reference Path

Resorting again to potential field methods, and being intuitive to bypass a given obstacle through the widest passageway, the algorithm presented in the previous section was used and four main scenarios were taken into account: the wider passage being free, the wider passage being obstructed, no wider passage and, lastly, no passage at all.

However, from the definition of the repulsive potential field, given by (22), and knowing that the repulsive force will have a direction perpendicular to the potential field that originated it, some problems were anticipated and four modifications were implemented, namely:

- 1) Track limits and obstacles were differentiated, meaning that they were defined by different repulsive fields;
- 2) The obstacles repulsive force was forced to have the direction of the vehicle's closest edge, instead of being perpendicular to the contour lines from the different danger levels;
- 3) The ability to check if a given obstacle is already behind was included (considering a given obstacle as passed when the CG is ahead of all the edges of the rectangle representing the obstacle);
- 4) The ability of change the repulsive and attractive gains if a collision is predicted (by projecting the current trajectory a fixed distance ahead) was incorporated;

Reference Speed

Since the approach followed for path planning requires an *a priori* knowledge about the track to obtain the speed profile, for obstacle avoidance this reference needs to be obtained with a different method which, in this work, was done resorting to

the concept of safety zones [9]. However, it should be noted that this method could also be used for path planning if there is no prior knowledge of the track layout.

This approach takes into account that any electromechanical system has an inherent response time, so the ability of a system to respond to a sudden obstacle can be derived from the concept of vehicle safety [9] and translated into the definition of multiple zones within the system observable environment. Such zones are four, which are represented in Figure 2, and are responsible for the velocity adjustment needed to avoid collision.

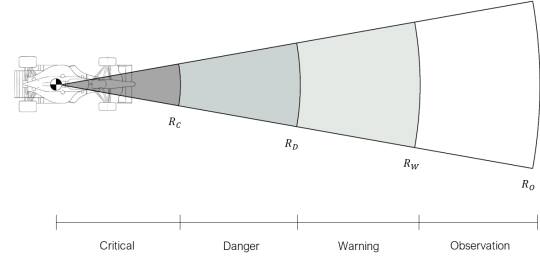


Figure 2. Schematic of the forces felt by the vehicle

Similarly to what was done for the reference path, some modification were implemented relatively to the concept typically found in the literature [9]:

- 1) Since a negative velocity is not allowed in FS competition, the profile was changed to take this constraint into account;
- 2) If no possible passage is detected, the reference speed is set to zero;
- 3) Due to possible chattering caused by a linear piecewise profile, a cubic spline interpolation were performed between the different radius, allowing a smooth transition between regions;
- 4) To avoid an "overshoot" in the observation zone, the velocity associated with this outer radius was slightly decreased from the maximum velocity;
- 5) The radius R_O , R_W and R_D were parameterised as function of velocity, with a linear relation, and not established as fixed values. R_C was fixed, containing the vehicle with an extra safety distance.

IV. DECOUPLED CONTROL APPROACH

The linearisation of the bicycle dynamics model with the tire slip ratio κ as additional state, provided in [4], shows clearly a division into two decoupled subsystems: a chained longitudinal subsystem; and a lateral subsystem. As such, for control purposes, a decoupled approach was followed developing the lateral and longitudinal controllers independently which will be presented in this section.

A. Longitudinal Control

As it was proposed in [4], a cascade control architecture with proportional gains was used. Such structure was chosen

as it allows to control the slip ratio and the longitudinal speed (chained variables) separately and perform a direct saturation of the physical quantities that must be limited. In this structure, the inner and outer loops variables are the slip ratio κ and the longitudinal speed v_x , respectively, since the former has a faster dynamics.

To take into account the load transfer occurring while the vehicle is describing a turn, a left/right motor torque asymmetry was created, assisting the control of the slip ratios generated in each tire, which is possible due to the use of independent wheel-hub motors. With this in mind, the control law implemented can be mathematically described by [4]

$$T_i = K_{\kappa}^i (\kappa_{\text{ref}} - \kappa_i - (-1)^i \kappa_{\text{diff}}) \quad (33)$$

where κ_{ref} and κ_{diff} can be computed as [4]

$$\kappa_{\text{ref}} = K_{v_x} (v_{x\text{ref}} - v_x) \quad (34a)$$

$$\kappa_{\text{diff}} = K_{\dot{\psi}} (\dot{\psi}_{\text{ref}} - \dot{\psi}) \quad (34b)$$

B. Lateral Control

The lateral control, related with the ability to steer the vehicle to a different lateral position, frequently relies on the knowledge of the vehicle's pose regarding the track, or in relation to a given referenced path, resorting to variables typically called path-following errors. As such, in this subsection these variables will be introduced first and then the control strategies will be presented.

Cross-track and Heading Errors

In autonomous driving it is essential to know the vehicle pose in relation to the track in order to allow the control algorithm to correct eventual errors. These can be related with a distance, like the cross-track error, or with an angle, which the heading error is an example of. Being possible to define such errors in different manners, in this work it was assumed that the vehicle had the waypoints in front of it, provided by the perception and planning algorithms, and would then curve fit them with a second-order polynomial in order to obtain a reference path [3].

The computation of the path-following errors under this assumption must be done in the absence or presence of a look-ahead distance L_{lad} since such concept is frequently used for control, as it allows for a timely correction of the errors, providing an anticipation capability. Considering \mathbf{p}_{RP} the closest point to the car, expressed in the local frame, and \mathbf{t}_{RP} the tangent at that point, since the only difference between using or not using a look-ahead distance is the location of this point and, consequently, the tangent (as it can be seen from Figure 3) the mathematical expression for the cross-track and heading error is the same regardless of the situation. Such computation can be given by [3]

$$e_y = \frac{\mathbf{p}_{RP} \times \mathbf{t}_{RP}}{\|\mathbf{t}_{RP}\|} \quad (35a)$$

$$e_{\psi} = \arcsin \left(\frac{\mathbf{t}_{RP} \times \mathbf{v}}{\|\mathbf{t}_{RP}\| \cdot \|\mathbf{v}\|} \right) \quad (35b)$$

where the heading error was defined as the angle between the referenced tangent and the vehicle's velocity vector \mathbf{v} to take into account eventual sideslip [3].

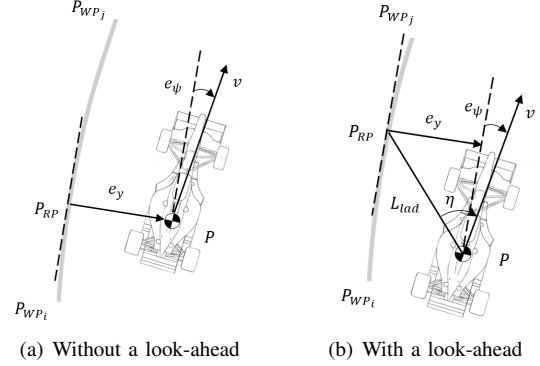


Figure 3. Cross-track and heading errors

An additional error parameter can also be defined, since it will be used in one of the controllers. Denoting it by η , it consists of the angle between the look-ahead vector (which can be obtained once the reference point as been established since its elements will be equal to the coordinates of such point in the local frame) and the velocity vector, as shown in Figure 3 (b). This variable can be computed as

$$\eta = \arcsin \left(\frac{\mathbf{v} \times \mathbf{p}_{RP}}{\|\mathbf{v}\| \cdot \|\mathbf{p}_{RP}\|} \right) \quad (36)$$

Control Strategies

→ Pure Pursuit (PP)

The Pure Pursuit controller [7] consists of a non-linear control strategy, where only one parameter is utilized as error, the angle η , represented in Figure 3 (b).

Assuming a kinematics vehicle model, and using a circular arc to connect the rear axle of the vehicle to an imaginary point moving along the desired path, this controller calculates the required steering angle from the curvature of such arc (obtained geometrically as shown in [7]) through the following law

$$\delta_{cmd} = \arctan \left(\frac{2L \sin(\eta)}{L_{lad}} \right) \quad (37)$$

→ Linear Quadratic Gaussian (LQG)

The Linear Quadratic Regulator (LQR) approach is a linear control strategy and it consists on minimising a given quadratic performance index [17] which penalises how far the final state of the system is from zero at the end of a finite time horizon and the state and control authority evolution during the same time horizon. For this minimisation, a significantly good approximation of the optimal solution can be obtained by solving the *Algebraic Riccati Equation* (ARE) [17] which requires establishing two tuning parameters: the state weighting matrix \mathbf{Q} , which penalises the deviation of the state from zero, and the control weighting matrix \mathbf{R} , which penalises the actuator authority.

Considering the bicycle dynamics model provided on Section II, the control law is given by [3]

$$\delta_{cmd} = -(K_y^{LQG} e_y + K_\psi^{LQG} e_\psi + K_{v_y}^{LQG} v_y + K_{\dot{\psi}}^{LQG} \dot{\psi}) \quad (38)$$

where the gains are obtained from the ARE. Since the model used is parameterised as a function of longitudinal velocity, these gains will be velocity dependent making it necessary to update them accordingly. This was done resorting to a gain scheduling, where the gains were calculated offline for the speed operating range and then obtained from a neighborhood table containing this values.

Since the variables v_y and $\dot{\psi}$ are not accessible directly from sensors, the design of a Kalman filter to estimate them is necessary. To obtain the gains related with this filter two additional parameters are needed, namely, the process \mathbf{Q}_0 and sensor \mathbf{R}_0 noise covariances. This estimator uses the same model as the one used for the LQR and resorts, once again, to a gain scheduling to update the gains.

For this work, the weighting matrices for the LQR and Kalman filter were:

$$\begin{aligned} \mathbf{Q}^{LQG} &= \text{diag}\{7, 15, 1, 1\}, \mathbf{R}^{LQG} = 5 \\ \mathbf{Q}_0^{LQG} &= \text{diag}\{0.5, 0.1, 0.1, 1\}, \mathbf{R}_0^{LQG} = \text{diag}\{0.01, 0.01\} \end{aligned}$$

→ Kinematics Lateral Speed (KLS)

The Kinematics Lateral Speed controller [7] bases itself on the distance between the vehicle and the reference path and on how such distance should influence the desired rate of change of the cross-track error \dot{e}_{y_d} : if the car is far from the reference line, it is required to make it get closer at higher rate than it would if it was close [7]. As such, \dot{e}_{y_d} can be defined as proportional to the cross-track error e_y , with negative sign. In order to reduce the error between the desired and actual rates of change, the controller must steer the car accordingly with [7]

$$\delta_{cmd} = \arctan \left(L \left(-K_\psi^{KLS} \sin(e_\psi) - \frac{K_\psi^{KLS} K_{e_y}^{KLS} e_y}{v_x} + \frac{k_{RP} \cos(e_\psi)}{1 - k_{RP} e_y} \right) \right) \quad (39)$$

where K_ψ^{KLS} and $K_{e_y}^{KLS}$ are positive constants and k_{RP} denotes the curvature of the path at the reference point \mathbf{p}_{RP} , which can be computed from a different definition to the one presented in (26), since a polynomial was used to curve fit a given set of waypoints. Considering x_i and y_i the coordinates expressed in the local frame of the n points curve fitted for the reference path generation and $f(x) = y = ax^2 + bx + c$ the function describing the second-order polynomial used, k_{RP} can be computed as

$$k_{RP} = \frac{2a}{(1 + (2ax_{RP} + b)^2)^{\frac{3}{2}}} \quad (40)$$

where the lower letter k was used since it is with respect to the local frame.

The gains used were $K_\psi^{KLS} = 1$ and $K_{e_y}^{KLS} = 2.5$.

This controller (and the next one) resorts to a bicycle vehicle model formulated with respect to the path to obtain, from linearisation, an general expression (provided in [7]) for the steering angle, which is then used to obtained the control laws.

→ Modified Sliding Mode (MSM)

The sliding mode strategy is a simple and robust control law which does not require a precise model of the system [7]. However, due to the discontinuous nature of its control action, this type of control usually leads to oscillations that are commonly designated as chattering which can be weakened or eliminated. As such, as suggested in [7], the sliding surface is defined as (41) and the sliding controller as (42) in order to ensure stability without chattering.

$$\sigma = K_{e_y} e_y + K_{e_\psi} e_\psi \quad (41)$$

$$\dot{\sigma} = -K_\sigma \sigma \quad (42)$$

The resulting Modified Sliding Mode control law can be obtained from [7]

$$\delta_{cmd} = \arctan \left(L \left(\frac{C_1}{v_x} + k_{RP} \frac{\cos(e_\psi)}{1 - k_{RP} e_y} \right) \right) \quad (43)$$

where K_{e_y} and K_{e_ψ} are weighting coefficients, k_{RP} is the curvature at the reference point computed from (40) and C_1 is given by

$$C_1 = - \frac{K_\sigma^{MSM} K_{e_y}^{MSM} e_y + K_\sigma^{MSM} K_{e_\psi}^{MSM} e_\psi + K_{e_y}^{MSM} \dot{e}_y}{K_{e_\psi}^{MSM}} \quad (44)$$

Since the variable \dot{e}_y is not accessible directly from sensors, a Kalman filter was designed to estimate it. The model used in this estimator was the bicycle dynamics one written in terms of road errors and, similarly to what was done in the LQG controller, resorts to a gain scheduling to update the gains.

The weighting matrices for the Kalman filter and the remaining gains used were:

$$\begin{aligned} \mathbf{Q}_0^{MSM} &= \text{diag}\{0.8, 0.5, 0.8, 0.5\}, \mathbf{R}_0^{MSM} = \text{diag}\{0.01, 0.01\} \\ K_\sigma^{MSM} &= 7, K_{e_\psi}^{MSM} = 0.1, K_{e_y}^{MSM} = 1. \end{aligned}$$

V. RESULTS AND DISCUSSION

Beginning with path planning, for evaluation purposes a track from the trackdrive event of a Formula Student competition held in Germany (FSG) was used. Such course is represented in Figure 4 along with the reference trajectory since the reference path is sketched with varying color, which has a correspondence to the values presented in the colorbar.

From the trajectory shown in Figure 4 it can be seen that the vehicle cuts corners while driving slower in corners and faster on straights; so the final solution captures the expected behaviour of a human driver. The parameters that allowed to obtain this solution are presented in Table I.

Since the use of the centerline is a typical baseline solution for the reference path, a comparison was made with this solution, which is presented in Table II. From this table it is possible to see that the centerline could lead to a considerable

loss of time in curves, which is mitigated with the method used since there is a tendency to cut corners.

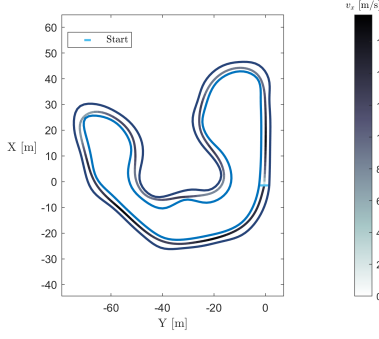


Figure 4. FSG reference trajectory

Table I. Planning parameters

Notation	Value	Units
K_{att}	1	N/m
K_{rep}	2	N
γ	10	-
offset	4	-
d_{offset}	6.16	m
d_{min}	0.75	m
Δs	1.50	m
η_{trans}	0.70	-
v_{xlim}	26.5	m/s

Table II. Comparison between centerline and the potential field solution

Reference path	t [s]	Improvement	
Centerline	30.86	-	-
Potential Field	27.00	3.86 [s]	12.50 [%]

Having been both reference path and speed profile obtained, the controllers performance in the trackdrive event can be evaluated recurring to suitable metrics. Considering that the reference path is intended to represent a solution closely to an optimal, the cross-track error is an important factor to take into account and, as such, the root-mean-square (RMS) of this error was used as an evaluation parameter. However, such error was computed separately to the one used for path-following, in order to guarantee an independent method to measure the distance to the reference path to be tracked. Knowing the curvature of the track and distinguishing a line from a arc of circumference if the curvature of the path between two waypoints has an absolute value below $0.002 \text{ [m}^{-1}\text{]}$, this error can be computed by [3]

$$e_y = \begin{cases} \frac{\mathbf{d}_{i,i+1} \times \mathbf{d}_{i,P}}{\|\mathbf{d}_{i,i+1}\|}, & \text{if } |K_{i,i+1}| < 0.002 \\ \text{sign}(R_{i,i+1}) \cdot (\overline{PC} - |R_{i,i+1}|), & \text{otherwise} \end{cases} \quad (45)$$

where C and $R_{i,i+1}$ are the center and radius of the circumference arc, respectively, $\mathbf{d}_{i,i+1}$ denotes the displacement vector from waypoint i to waypoint $i+1$ and $\mathbf{d}_{i,P}$ the displacement between a waypoint i and the reference point in the car P .

Lastly, noting that some of the implemented control strategies require or could benefit from the use of a look-ahead distance, and keeping in mind that such distance should change with the longitudinal speed, the performance for such

controllers was evaluated for two types look-ahead profiles, namely a linear and a parabolic one, both present in (46).

$$L_{lad_1} = 1 + 0.25v_x \quad (46a)$$

$$L_{lad_2} = \left(\frac{v_x}{5}\right)^2 \quad (46b)$$

The results for this event are presented in Table III where a column was added to provide additional information. This column qualitatively informs if, in the path actually described, the vehicle touched the cones, but still managed to remain in the track (being signaled a penalty) or if the vehicle did not finish the course (which will be shown as DNF).

Table III. Trackdrive results

Controller	L_{lad}	RMS(e_y) [m]	Penalty
PP	1	0.05	-
	2	0.07	-
LQG	1	0.04	-
	2	-	DNF
KLS	-	0.05	-
MSM	-	0.10	-

Beginning the analysis with the cross-track error, it can be highlighted that the PP, LQG and KLS controllers present a similar performance being the difference between the MSM and these controllers not significant and possibly diminished with further tuning. Although not presented, some tests were performed using the centerline as reference path and it was noted that the cross-track error increased. Such phenomenon can be explained by the general increase of the curvature, making it harder to track with the same precision as in the path used. Regarding the look-ahead analysis, the most clear conclusion is that the linear profile enables both controllers to finish the track and allows for a better performance, with respect to the cross-track error. This can be explained by how the speed influences this predictive distance. The variation in the parabolic profile is more significant, which means that it will result in higher values for the distance, leading the controllers to correct their position prematurely and, consequently, losing part of the benefit associated with this concept. This occurrence is in accordance with what usually happens in the behaviour of a driver: being the predictive distance dependent not only on speed, but also on curvature, it is usually smaller for larger curvatures, which can be better achieved with the linear profile used as it presents, in general, lower values.

Analysing now the obstacle avoidance scenario, the break-points used are presented in Table IV and the results can be found in Figure 5. Regarding steering, the vehicle is still able to portray what can be considered as an expected path, but some "clumsy" movements can be detected. However, this occurs mostly in tight curves and the vehicle still manages to perform them and remain within the track. On the other hand, the behaviour regarding speed presents less flaws, since the speed is decreased in the proximity of an obstacle or in a curve, but increased in straights, as expected. The minimum distance to track limits and obstacles were also computed and it was found that the vehicle complete the track without touching

boundaries or obstacles. However, a difficulty in guaranteeing a trajectory without collision was verified (using other tracks and obstacles layouts), meaning that the developed algorithm is difficult to generalise.

Table IV. Points used for cubic spline interpolation where $v_{x_{\max}} = 15$ [m/s]

	R_O	R_W	R_D	R_C
Distance [m]	$1.5 v_x$	$1.2 v_x$	$0.9 v_x$	$1.5 L$
Velocity [m/s]	$v_{x_{\max}}$	$v_{x_{\max}} - 3$	$v_{x_{\max}}/2 - 1$	0

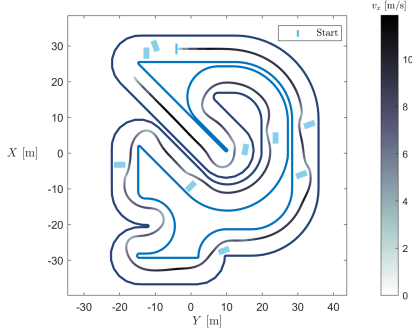


Figure 5. Obstacle avoidance results

Weighting all comments and results it was considered that the different control strategies implemented correspond to adequate solutions for vehicle guidance and that the planning algorithms are able to provide a satisfactory solution.

VI. CONCLUSIONS

Analysing the results documented in the previous section, it can be concluded that the objectives of this work were accomplished. Regarding planning, the adopted approaches do not guarantee optimality, but are able to portray the expected behaviour of a human driver. With respect to control, a set of controllers and path-following strategies was provided, enabling a FS vehicle to follow a given path.

However, some improvements could be implemented in future work. Relatively to simulation, some realistic models for the sensors and a mechanism that simulates the perception algorithms could be included. Regarding planning, formulations that allow to simultaneously optimises the path and speed profile should be investigated. In addition, if such reference is obtained in an offline fashion, some mechanism for online update should be present since the actual conditions may not match those expected when the reference was generated. Lastly, for obstacle avoidance, approaches that allow a coupling between the lateral and longitudinal subsystems should be analysed and dynamic obstacle should be considered.

ACKNOWLEDGMENT

The author would like to thank professors Duarte Valério, José Raul Azinheira, Miguel Ayala Botto and Alexandra Moutinho, as well as André Barroso and Alexandre Athayde for all the help and availability in this work.

REFERENCES

- [1] L. Andresen, A. Brandemuehl, A. Honger, B. Kuan, N. Vodisch, H. Blum, V. Reijgwart, L. Bernreiter, L. Schaupp, J. Chung, M. Bürki, M. Oswald, R. Siegwart, and A. Gawel. Accurate mapping and planning for autonomous racing. In *2020 IEEE/RSJ International Conference on Intelligent Robots and Systems (IROS)*, pages 4743–4749, 10 2020.
- [2] J. Antunes. Torque vectoring for a formula student prototype. Master's thesis, IST, 2017.
- [3] A. Athayde. Path following and control for autonomous driving of a formula student car. Master's thesis, IST, 2021.
- [4] A. Barroso. Traction control of a formula student prototype. Master's thesis, IST, 2021.
- [5] R. Cordeiro. Modelagem e controle de trajetória de um veículo robótico terrestre de exterior. Master's thesis, UNICAMP, 2013.
- [6] R. De Angelis Cordeiro, J. Azinheira, E. Paiva, and S. Bueno. Dynamic modeling and bio-inspired lqr approach for off-road robotic vehicle path tracking. In *2013 16th International Conference on Advanced Robotics (ICAR)*, pages 1–6, 11 2013.
- [7] S. Dominguez, A. Ali, G. Garcia, and P. Martinet. Comparison of lateral controllers for autonomous vehicle: Experimental results. In *2016 IEEE 19th International Conference on Intelligent Transportation Systems (ITSC)*, pages 1418–1423, 2016.
- [8] J.-F. Duhé, S. Victor, and P. Melchior. Contributions on artificial potential field method for effective obstacle avoidance. *Fractional Calculus and Applied Analysis*, 24(2):421–446, 2021.
- [9] A. Ferreira. Teleoperation with force feedback: Easing unmanned vehicles operation in unknown scenarios. Master's thesis, IST, 2015.
- [10] J. Filip. Trajectory tracking for autonomous. Master's thesis, Czech Technical University in Prague, 2017/2018.
- [11] M. Gerds, S. Karrenberg, B. Müller-Beßler, and G. Stock. Generating locally optimal trajectories for an automatically driven car. *Optimization and Engineering*, 10:439–463, 12 2009.
- [12] D. Gonzalez Bautista, J. Pérez, V. Milanés, and F. Nashashibi. A review of motion planning techniques for automated vehicles. *IEEE Transactions on Intelligent Transportation Systems*, pages 1–11, 11 2015.
- [13] J. Kabzan, M. I. Valls, V. Reijgwart, H. F. C. Hendrikx, C. Ehmke, M. Prajapat, A. Bühler, N. Gosala, M. Gupta, R. Sivanesan, A. Dhall, E. Chisari, N. Karnchanachari, S. Brits, M. Dangel, I. Sa, R. Dubé, A. Gawel, M. Pfeiffer, A. Liniger, J. Lygeros, and R. Siegwart. Amz driverless: The full autonomous racing system. *ArXiv*, abs/1905.05150, 2020.
- [14] J. Kong, M. Pfeiffer, G. Schilbach, and F. Borrelli. Kinematic and dynamic vehicle models for autonomous driving control design. In *2015 IEEE Intelligent Vehicles Symposium (IV)*, pages 1094–1099, 2015.
- [15] M. Laurenza, G. Pepe, D. Antonelli, and A. Carcaterra. Car collision avoidance with velocity obstacle approach: Evaluation of the reliability and performance of the collision avoidance maneuver. In *2019 IEEE 5th International forum on Research and Technology for Society and Industry (RTSI)*, pages 465–470, 2019.
- [16] A. Liniger. *Path Planning and Control for Autonomous Racing*. PhD thesis, ETH Zurich, 2018.
- [17] K. Ogata. *Modern Control Engineering*. Prentice Hall, 5th edition, 2009.
- [18] H. B. Pacejka and E. Bakker. The magic formula tyre model. *Vehicle System Dynamics*, 21(sup001):1–18, 1992.
- [19] S. Pendleton, H. Andersen, X. Du, X. Shen, M. Meghjani, Y. Eng, D. Rus, and M. Jr. Perception, planning, control, and coordination for autonomous vehicles. *Machines*, 5:6, 02 2017.
- [20] R. Rajamani. *Vehicle Dynamics and Control*. Springer, 2nd edition, 2012. ISBN:978-1461414322.
- [21] W. Schwarting, J. Alonso-Mora, and D. Rus. Planning and decision-making for autonomous vehicles. *Annual Review of Control, Robotics, and Autonomous Systems*, 1, 05 2018.
- [22] P. Torino. Combined lateral and longitudinal control for autonomous driving based on model predictive control. Master's thesis, Politecnico Di Torino, 2019.
- [23] D. Valério and J. Costa. *An Introduction to Fractional Control*. The Institution of Engineering and Technology, 2013. ISBN:978-1-84919-546-1.
- [24] J. Van Brummelen, M. O'Brien, D. Gruyer, and H. Najjaran. Autonomous vehicle perception: The technology of today and tomorrow. *Transportation Research Part C: Emerging Technologies*, 89, 03 2018.